
On the Sample Efficiency of Abstractions and Potential-Based Reward Shaping in Reinforcement Learning

Giuseppe Canonaco¹ Leo Ardon¹ Alberto Pozanco¹ Daniel Borrajo¹

Abstract

The use of Potential Based Reward Shaping (PBRs) has shown great promise in the ongoing research effort to tackle sample inefficiency in Reinforcement Learning (RL). However, the choice of the potential function is critical for this technique to be effective. Additionally, RL techniques are usually constrained to use a finite horizon for computational limitations. This introduces a bias when using PBRs, thus adding an additional layer of complexity. In this paper, we leverage abstractions to automatically produce a "good" potential function. We analyse the bias induced by finite horizons in the context of PBRs producing novel insights. Finally, to assess sample efficiency and performance impact, we evaluate our approach on four environments including a goal-oriented navigation task and three Arcade Learning Environments (ALE) games demonstrating that we can reach the same level of performance as CNN-based solutions with a simple fully-connected network.

1. Introduction

Reinforcement Learning (RL) is able to achieve impressive results at the cost of requiring a huge amount of samples (Silver et al., 2018; Vinyals et al., 2019; OpenAI et al., 2019). This sample inefficiency prevents RL to be more widely applied into the real world because of the cost that can be associated to experience collection, ultimately demanding the development of algorithms able to counteract or at least mitigate this issue.

In the RL literature, we can find many different methods to tackle the above-mentioned problem among which we have Transfer Learning (Taylor & Stone, 2009), zero-shot RL (Touati et al., 2022), or variance reduction techniques (Papini et al., 2018). Yet another promising way to

compensate for the widely known sample inefficiency of RL is through abstractions. For instance, Hierarchical RL (HRL) (Hutsebaut-Buyse et al., 2022) is a sub-field aiming at leveraging compositionality through learning reusable sub-behaviours which, in turn, are combined together via a higher level strategy. Thus, HRL is able to produce better sample efficiency through behavioral abstraction.

Instead of focusing on behavioral abstractions, an entire branch of RL focuses on building abstractions of Markov Decision Processes (MDPs) (Puterman, 2014). An MDP is the mathematical formalism commonly used to model an RL problem. Abstractions of MDPs aim at reducing the state space size of the original problem to transform the search for a solution into a simpler task. Examples of such techniques are Weighting Function Abstractions (Li et al., 2006), Abstract Robust MDPs (Petrik & Subramanian, 2014), and Abstract Bounded Parameter MDPs (Givan et al., 2000). These techniques strive to work directly on the aggregated state space to produce a solution for the original problem. However, the stochastic process over the aggregated space turns out to be a Partially Observable MDP (POMDP) (Bai et al., 2016) and approximating a non-Markovian process with Markov dynamics can likely result in poor performance.

An alternative way to leverage abstractions consists in using them for Potential-Based Reward Shaping (PBRs) (Ng et al., 1999). Reward shaping uses an auxiliary function, called potential, to provide additional feedback to the agent and improve sample efficiency. Abstractions can be used to automatically generate a potential function for reward shaping producing a guide for more focused exploration when learning the optimal policy on the original task. This idea has been recently introduced in the literature. Indeed, Cipollone et al. (2023) compute the solution of an abstraction, the optimal value function, and use it as a potential function for reward shaping. They focus on goal-oriented MDPs. Additionally, when dealing with RL problems in practice the horizon length cannot be infinite, hence reward shaping has an intrinsic bias (Grzes, 2017). For this reason, Cipollone et al. (2023) propose an off-policy scheme in order to avoid problems of convergence to the optimum of the original task due to this bias. This scheme

¹JP Morgan AI Research. Correspondence to: Giuseppe Canonaco <giuseppe.canonaco@jpmorgan.com>.

has a doubled computational complexity because updates need to be done for two different agents.

In this paper, we study the above-mentioned bias theoretically both in the context of goal-oriented and general MDPs to understand how to control it, and what impact it may have on policy ordering in the reshaped MDP w.r.t. the original problem. We will also show experimentally how abstractions coupled with PBRS can make a significant difference in terms of sample efficiency in the Arcade Learning Environment (ALE) benchmark (Bellemare et al., 2013) achieving performances comparable or superior to the ones of Convolutional Neural Networks (CNNs) (Mnih et al., 2015), but only using fully-connected architectures. To the best of our knowledge, this is unprecedented.

2. Background

In the RL setting, an agent interacts with the environment to learn a policy. After perceiving the current state of the environment, the agent executes an action that makes the environment transition into a next state. Finally, the agent collects the reward associated to the experienced transition and the cycle starts again. Problems in the RL paradigm are usually modeled through MDPs. An MDP is described as a tuple $\{\mathcal{S}, \mathcal{A}, \mathcal{P}, r, \gamma, \rho\}$, where \mathcal{S} is the state space, \mathcal{A} is the action space, $\mathcal{P}(s'|s, a)$ is the Markovian state transition function, $r(s, a, s') \in [0, \bar{R}]$ is the reward function, $\gamma \in [0, 1)$ is the discount factor, and ρ is the initial state distribution.

Techniques to solve an RL problem can be divided into Value-based and Policy-based algorithms. The former ones strive to learn the optimal (action) value function $V^*(s)$ ($Q^*(s, a)$), whereas the latter ones aim at directly learning the optimal policy. The optimal action value function $Q^*(s, a)$ is defined as the expected obtained return starting in state s , executing action a , and following the optimal policy thereafter. Instead, the optimal value function $V^*(s)$ can be obtained starting from $Q^*(s, a)$ and selecting a according to the optimal policy, or, equivalently, selecting a greedily w.r.t. $Q^*(s, a)$. This means that $V^*(s) = \max_a Q^*(s, a)$ and that the optimal policy can be obtained by acting greedily on the environment under the guidance of the optimal action value function.

While the approach presented in this paper is agnostic to any characteristic of the RL algorithm, we have performed experiments using Deep Q-Networks (DQNs) (Mnih et al., 2015). Given a data set of collected experience $D = \langle s_t, a_t, r_t, s_{t+1} \rangle_{t=1}^N$, during learning, a DQN minimizes the following loss function leveraging samples of experience drawn uniformly at random from D :

$$\mathbb{E}_{(s,a,r,s') \sim D} \left[\left(r + \gamma \max_{a'} Q_{\theta^-}(s', a') - Q_{\theta}(s, a) \right)^2 \right],$$

where Q_{θ} and Q_{θ^-} are action value functions parameterized by the vector of weights θ and θ^- represented by CNNs (LeCun et al., 1998). They respectively represent the actual action value function and the target action value function. The former is always updated whereas the latter is only updated every C steps.

2.1. Potential-Based Reward Shaping

The idea behind PBRS (Ng et al., 1999) is to help the agent with additional reward feed-back to steer the learning process towards paths that reach optimal behaviour faster. This is accomplished by running the learning algorithm on $\mathcal{M}' = \{\mathcal{S}, \mathcal{A}, \mathcal{P}, r', \gamma, \rho\}$, a different MDP, called the reshaped MDP, where $r'(s, a, s') = r(s, a, s') + F(s, a, s')$. If $F(s, a, s') = \gamma\phi(s') - \phi(s)$, where $\phi : \mathcal{S} \rightarrow \mathbb{R}$ is bounded and the horizon length, H , is infinite, we are guaranteed that the optimal policy in \mathcal{M}' is optimal also in \mathcal{M} (this holds also for ϵ -optimal policies). The potential ϕ can be interpreted as a guide telling the agent how valuable a certain state is. Furthermore, this reshaping approach implies the following relationship between value functions (and analogously for action-value functions): $\mathcal{V}_{\mathcal{M}'}^{\pi} = \mathcal{V}_{\mathcal{M}}^{\pi} - \phi$ (Ng et al., 1999).¹

Unfortunately, in practice, RL algorithms cannot solve a problem using an infinite horizon, which implies setting a limit to $H < \infty$. This, in turn, implies a bias that comes from the fact that the reshaped return depends on the final state reached by the agent (Grzesi, 2017):

$$\mathcal{R}'(\tau) = \mathcal{R}(\tau) + \gamma^H \phi(s_H) - \phi(s_0), \quad (1)$$

where τ is a trajectory and $\mathcal{R}(\tau) = \sum_{t=0}^{H-1} \gamma^t r(s_t, a_t, s_{t+1})$ is the discounted return. Since the last visited state depends also on the policy it is clear that optimizing $\mathcal{R}'(\tau)$ is not the same as optimizing $\mathcal{R}(\tau)$.

3. Sample Efficiency Through Abstractions and PBRS

When using PBRS, we need to select a good potential $\phi(s)$. It is known that using the optimal value function for the task at hand represents a good choice. Hence, it is common to use handcrafted heuristics in an attempt to approximate the optimal value function of the original task to perform the reshaping (Ng et al., 1999). However, instead of using handcrafted functions, leveraging some available knowledge, we could define an abstraction of the task at hand that,

¹The dependency on the state has been neglected for readability.

once solved, will provide us with an optimal value function to be used as potential. This idea works under the intuition that the abstraction should be a simplified version of the original task whose solution should provide an estimate of the original task’s optimal value function. Furthermore, in many tasks, it is way easier for a human to provide knowledge via the definition of a simpler task rather than through the definition of a specific potential function.

Formally, let $\alpha(s) : \mathcal{S} \rightarrow \bar{\mathcal{S}}$ be an aggregation function mapping each state of the original task into a state in $\bar{\mathcal{S}}$, representing the state space of the user-defined abstraction, with $|\bar{\mathcal{S}}| \ll |\mathcal{S}|$. Also, let $\bar{V}^*(\bar{s})$ be the optimal value function of the abstraction. Then, in the context of this work, we will perform reshaping in the following manner:

$$r'(s, a, s') = r(s, a, s') + \gamma \bar{V}^*(\alpha(s')) - \bar{V}^*(\alpha(s)), \quad (2)$$

where $\phi(s) = \bar{V}^*(\alpha(s))$.

The benefit of PBRS can be seen immediately in sparse reward settings, where we densify the reward through the aid of the potential, making the exploration phase easier for the agent. However, let us consider more general settings. We start analyzing the performance impact of PBRS on the Value Iteration (VI) algorithm.

Proposition 3.1 (VI Performance). Given an MDP \mathcal{M} , a potential function ϕ , an initialization point V_0 , and assuming that $\|\mathcal{V}_{\mathcal{M}}^* - \phi - \mathcal{V}_0\|_{\infty} \leq \|\mathcal{V}_{\mathcal{M}}^* - \mathcal{V}_0\|_{\infty}$ (it can be made true if ϕ is an approximation of $\mathcal{V}_{\mathcal{M}}^*$), then, by applying VI starting from \mathcal{V}_0 in both the original and reshaped MDP, the minimum number of iterations to guarantee ϵ -optimality in the reshaped MDP will be lower than in the original MDP.

Proof. Applying VI in the original MDP \mathcal{M} , where $\mathcal{V}_{n,\mathcal{M}}^{src}$ is the output after n iterations, yields the following bound by the γ -contraction property:

$$\|\mathcal{V}_{\mathcal{M}}^* - \mathcal{V}_{n,\mathcal{M}}^{src}\|_{\infty} \leq \gamma^n \|\mathcal{V}_{\mathcal{M}}^* - \mathcal{V}_0\|_{\infty}. \quad (3)$$

Applying VI in the reshaped MDP \mathcal{M}' , where $\mathcal{V}_{n',\mathcal{M}'}^{dst}$ is the output after n' iterations brought back into the original MDP through **Corollary 2** in (Ng et al., 1999), yields the following bound by the γ -contraction property:

$$\|\mathcal{V}_{\mathcal{M}}^* - \phi - \mathcal{V}_{n',\mathcal{M}'}^{dst} + \phi\|_{\infty} \leq \gamma^{n'} \|\mathcal{V}_{\mathcal{M}}^* - \phi - \mathcal{V}_0\|_{\infty}. \quad (4)$$

Then, since

$$\|\mathcal{V}_{\mathcal{M}}^* - \phi - \mathcal{V}_0\|_{\infty} \leq \|\mathcal{V}_{\mathcal{M}}^* - \mathcal{V}_0\|_{\infty} \quad (5)$$

thanks to ϕ , VI applied on the reshaped problem will require a smaller minimum number of iterations to guarantee an ϵ -optimal solution. Notice that, the superscripts *src* and *dst* are used to disambiguate the two solutions of VI that may be different. \square

Proposition 3.1 tells us that improvements are achievable in the context of Value Iteration whenever we are able to provide a good estimate of the optimal value function through the potential function in the PBRS technique. However, this grants us just computational savings, and we would like to convert it into a greater sample efficiency in the context of a general RL setting.

For what concerns value-based algorithms like Q-Learning (Watkins & Dayan, 1992) and SARSA (Rumery & Niranjan, 1994), Wiewiora (2003) showed that, under the assumption of learning through the same experience, PBRS is equivalent to initializing the action-value function with the potential function. This can be interpreted as a very naive form of Transfer Learning (Taylor & Stone, 2009; Lazaric, 2012). Hence, whenever initializing the action-value function with a potential function that represents a good starting estimate of the optimal solution, we will observe a greater sample efficiency. Furthermore, additional insights on this technique in the context of RL can be gained through **Proposition 3.2**:

Proposition 3.2 (Baseline Equivalence). In the context of the Policy Gradient Theorem (Sutton et al., 1999), using PBRS is equivalent to using a baseline $b(s) = \phi(s)$.

Proof. Applying the Policy Gradient Theorem to the reshaped MDP \mathcal{M}' :

$$\nabla_{\theta} J_{\theta} = \sum_s d^{\pi_{\theta}}(s) \sum_a \pi_{\theta}(a|s) \nabla_{\theta} \log \pi_{\theta}(a|s) \mathcal{Q}_{\mathcal{M}'}^{\pi_{\theta}}(s, a), \quad (6)$$

where $d^{\pi_{\theta}}(s) = \sum_{t=0}^{\infty} \gamma^t Pr\{s_t = s | s_0, \pi_{\theta}\}$. Now, using **Corollary 2** in (Ng et al., 1999), we get:

$$\sum_s d^{\pi_{\theta}}(s) \sum_a \pi_{\theta}(a|s) \nabla_{\theta} \log \pi_{\theta}(a|s) (\mathcal{Q}_{\mathcal{M}'}^{\pi_{\theta}}(s, a) - \phi(s)) \quad (7)$$

If we combine Eq. 7 with $b(s) = \phi(s)$, it yields the baseline version of the Policy Gradient Theorem. In the case of finite horizons, we are forced to use a non-stationary potential (Devlin & Kudenko, 2012) as proposed by Grzes (2017) (which is unbiased), so that $\phi(s_H) = 0$ and the Monte-Carlo estimate of $\mathcal{Q}_{\mathcal{M}'}^{\pi_{\theta}}(s, a)$ can be decomposed as above.²

\square

It is widely known that using value function estimates as baselines allows Policy Gradient algorithms to suffer less variance in its gradients (Schulman et al., 2015). This, in turn, implies a greater sample efficiency because of the more precise direction estimate toward which the algorithm

² $\phi(s_H) = 0$ only for the states encountered at the end of a trajectory. If the same state is encountered before, its original potential is used.

will move during its optimization process. Since *Proposition 3.2* shows the equivalence between baselines and PBRS, we can deduce that a good value function estimate provided by the potential will help us in our goal of improving sample efficiency, achieving better performance. The main advantage of using PBRS is that it is not mandatory to estimate the value function from data collected by the agent. Instead, the estimate may come from a simplified representation of the problem the agent is tackling. This enables a different way to provide knowledge to the agent while learning and does not require the representation to be perfect, easing the user from the burden of providing accurate models.

4. Bias Analysis

Now, we focus on the bias induced by PBRS in the episodic setting. We will start by considering goal-oriented MDPs, and then we will focus on general MDPs to understand the conditions under which policy ordering is preserved between the original problem and the reshaped one.

Theorem 4.1 (Policy Ordering in Goal-Oriented Episodic MDPs). In the episodic context, let \mathcal{M} be a goal-oriented MDP and \mathcal{M}' be its reshaped version obtained using a bounded potential. Then, the policy ordering in \mathcal{M} is preserved in the reshaped MDP \mathcal{M}' for all the policies reaching the goal in at most H steps.

In a goal-oriented MDP, whenever we fix an horizon length for computational reasons, we are setting a limit on the sensitivity of our agent. Indeed, policies reaching the goal in $H + 1$ steps cannot be distinguished among policies reaching the goal in more than $H + 1$ steps. Bearing this in mind, the above Theorem (proof in Appendix A.1), tells us that, as long as the goal can be reached in at most H steps, then the reshaped problem is equivalent to the original one. This conclusion has good practical implications, because it allows PBRS to be used without taking care of the bias due to Eq. (1), avoiding computationally expensive approaches like the off-policy scheme proposed by Cipolone et al. (2023). In the context of general MDPs, we can give a condition under which the policy ordering is preserved across the two problems.

Theorem 4.2 (Policy Ordering in Reshaped Episodic MDPs). Let \mathcal{M} be an MDP and \mathcal{M}' be its reshaped version obtained using a bounded potential $\phi : \mathcal{S} \rightarrow [0, \Phi]$. Then, there exists an horizon

$$H > \log_{\gamma} \inf_{\substack{\pi_A, \pi_B: \\ \mathbb{E}_{\rho}[V^{\pi_A}(s)] > \mathbb{E}_{\rho}[V^{\pi_B}(s)]}} \frac{\mathbb{E}_{\rho}[V^{\pi_A}(s)] - \mathbb{E}_{\rho}[V^{\pi_B}(s)]}{\Phi + \frac{\bar{R}}{1-\gamma}}$$

such that the ordering in the reshaped MDP is preserved w.r.t. the infinite-horizon version of \mathcal{M} .

The condition reported by Theorem 4.2 (proof in Ap-

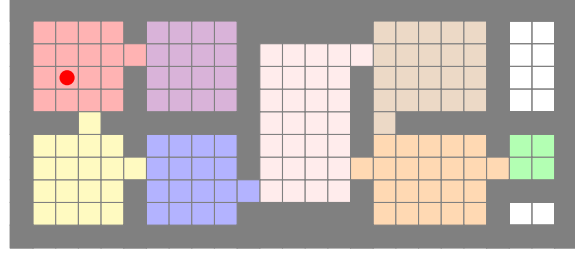


Figure 1: 8-rooms task. The agent is depicted as a red dot, the goal is represented in green, and the gray blocks represent the walls. Each color also represents a macro-state exhaustively defining the aggregation function.

pendix A.2) is very restrictive, because preserving the total ordering of policies is a strong equivalence requirement. The least restrictive version of total ordering is preserving only the optimal policy which is considered in the following Corollary.

Corollary 4.3 (Preserving the Optimal Policy in Reshaped Episodic MDPs). Let \mathcal{M} be an MDP and \mathcal{M}' be its reshaped version obtained using a bounded potential $\phi : \mathcal{S} \rightarrow [0, \Phi]$. Then, there exists a horizon

$$H > \log_{\gamma} \frac{\mathbb{E}_{\rho}[V^{\pi^*}(s)] - \mathbb{E}_{\rho}[V^{\pi^{**}}(s)]}{\Phi + \frac{\bar{R}}{1-\gamma}},$$

where π^{**} is the second-best policy, such that the optimal policy in the reshaped MDP is equivalent to the one in the infinite-horizon version of \mathcal{M} .

Proof. It is enough to select $\pi_A = \pi^*$ in Theorem 4.2. This implies that π_B must be π^{**} . \square

Now, the horizon length depends on the difference between the performance associated to the optimal policy and the performance of the second best policy, which is way less stringent than what stated in Theorem 4.2.

5. Evaluation

In this section, we experimentally evaluate the impact of abstractions coupled with PBRS on sample efficiency. This will be accomplished in the context of a goal-oriented navigation task and some complex ALE games.

5.1. Grid World

In order to corroborate all the theoretical findings about goal-oriented MDPs described in the previous section, we evaluate the performance of the Q-Learning algorithm, coupled with the reshaping described in Equation 2, against the Q-Learning-based off-policy approach

proposed by Cipollone et al. (2023). This comparison was done over the 8-rooms goal-oriented navigation task (Cipollone et al., 2023) depicted in Figure 1. The agent has to move from the top-left room to the right-most one in order to accomplish the task. The abstraction consists in considering only the rooms and their connections (see Appendix B.1). Further experimental details may be found in Appendix C.

Figure 2a shows how reshaping according to Equation 2 has better performance than Cipollone et al. (2023) proposed solution. This is due to the fact that the bias introduced by the reshaping is non-existent in finite-horizon goal-oriented MDPs, as shown in Theorem 4.1. We have also reported vanilla Q-Learning performance for completeness.

5.2. Arcade Learning Environment

We also show how our approach behaves in way more challenging tasks, ALE games (Bellemare et al., 2013). We have chosen three tasks of increasing level of difficulty and significantly different among each other in terms of dynamics: *Freeway*, *Q*Bert*, and *Venture*. In *Freeway*, the agent needs to cross a road avoiding the cars driving along the 10 different lanes. Every time the agent bumps into a car, it will get thrown backward a few steps, whereas upon crossing the entire road it will get one point and restart from the beginning. The game lasts 2 minutes and 16 seconds and the overall objective is to cross the entire road as many times as possible.

In *Q*Bert*, the agent can jump onto some tiles over a grid. Jumping onto tiles the agent is able to change their color. The goal of the agent is to change every tile on the grid to a target color of interest. This will make it succeed and go to the next level. The agent is awarded 25 points for each tile turned to the target color. Furthermore, it is awarded a bonus of 3100 points on level completion. Unfortunately, while the agent attempts to accomplish its task, there are enemies attempting at its life or undoing its tile-coloring work.

Finally, in *Venture*, the agent is placed into a main hall that has to be explored in order to find some rooms where treasures have been hidden. In order to progress, the agent has to enter each room, collect its treasure, and exit the room without being killed by the enemies and pitfalls present in every room (including the main hall). The agent will receive 200 points for each collected treasure and 100 points for each killed enemy in the treasure rooms (these last points are awarded only if the killing happens after the treasure has been collected). This reward system makes the task a sparse reward problem, which is way harder to deal with for RL agents.

To tackle the above described tasks, we will use DQN (a gist of the algorithm can be found in Section 2). In the experiments, we will compare DQN based on fully-connected architectures against the same algorithm, but this time applied on a reshaped environment, where the reshaping is based on Equation 2. This is done to evaluate the contribution of the abstraction on sample efficiency. Due to the complexity of the tackled tasks, we will try to adhere as much as possible to theory. However, deviations from it will be allowed whenever these make the implementation feasible or they yield better performance (implementation details in Appendix B). The previously mentioned algorithms, using fully-connected neural networks as value function estimators, have been trained on the RAM version of the above mentioned ALE games. This implies that the state space of those environments will be represented by a 128-dimensional vector whose components may take up to 256 values encoding various different information about the current state of the game (e.g., coordinates of the agent, coordinates of the enemies, etc.). To further assess the contribution over sample efficiency and performance achievable through the abstractions, we will additionally compare the fully-connected version of DQN against its CNN version first introduced by Mnih et al. (2015). DQN based on CNN architectures will be trained straight from images (the more classical representation of the state space in ALE).

Before diving into the results, we will briefly describe the abstractions for the above-mentioned ALE games. Each one of them has been developed by simplifying the game via neglecting enemies or entire areas/dynamics of the game itself.

5.2.1. ABSTRACTING FREEWAY

Freeway represents the simplest task we tackled in the context of the ALE benchmark because fully-connected neural networks are able to achieve more than 85% of the CNNs performance on their own. In this task, we propose a very simple abstraction where we neglect the presence of the cars and we model a simple empty road to be crossed by the agent. The agent starts at position 6 (only the y coordinate is considered because the agent cannot move horizontally) and has to cross position 180 by moving up, down, or doing nothing (1,2, and 0, respectively). Movement actions will increment or decrement the position of the agent by 1 in the respective direction. Since there are no cars in this abstraction, it is pointless to maximize the amount of times the agent crosses the road; it is sufficient to consider just one crossing. This abstraction has 177 states and its aggregation function is the following:

$$\begin{aligned} \alpha_{s,s'}(s) &= (s_{14}, 0) \\ \alpha_{s,s'}(s') &= (s'_{14}, s'_{103} - s_{103}), \end{aligned}$$

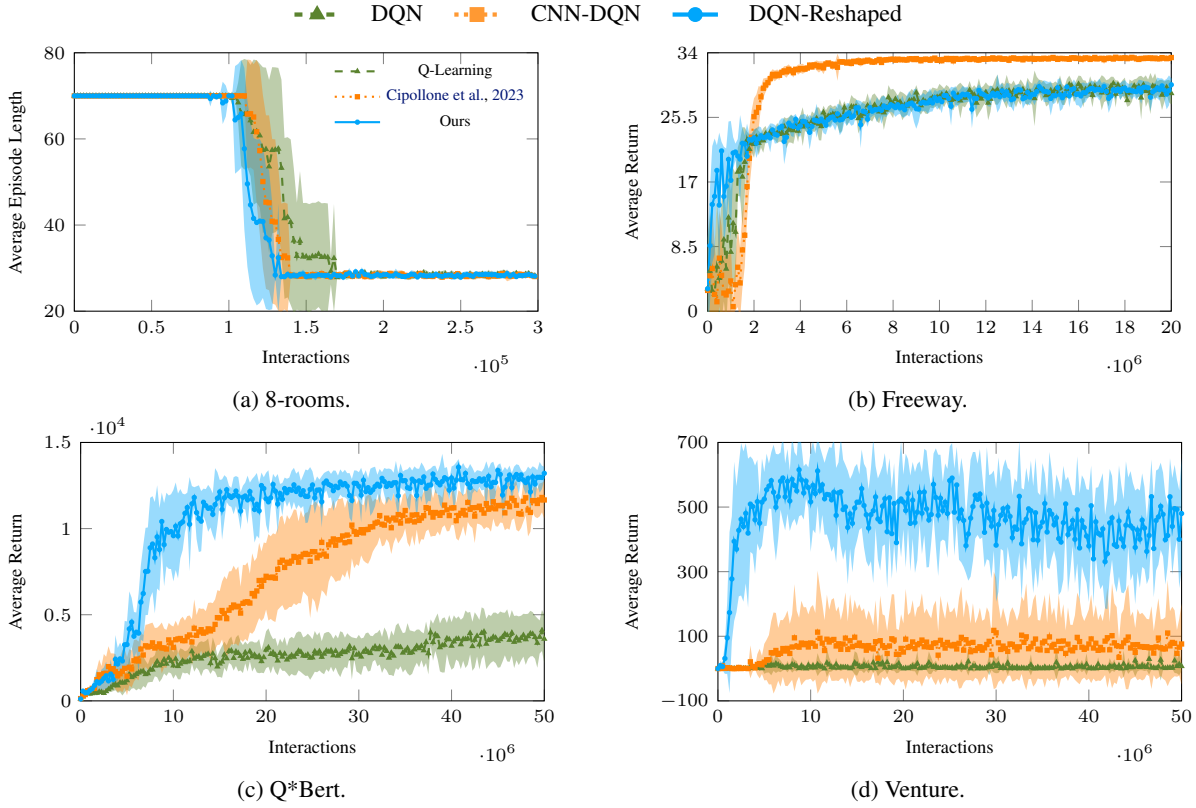


Figure 2: Average return ± 1 standard deviation achieved by the algorithms computed using 10 independent runs in all the selected environments.

where we have used the 14th and 103rd coordinates (y and score, respectively (Anand et al., 2019)) of the RAM vector representing the state space of the original task. This aggregation function allows us to deal with a smaller abstraction because we do not have to consider multiple crossing of the whole road, but only one. Finally, this proposed abstraction is solved through VI and its solution is used to perform reshaping on the original task as per Equation 2.

5.2.2. ABSTRACTING Q*BERT

In order to abstract away what the agent has to accomplish in *Q*Bert*, we neglect all the enemies and consider only the positions of the tiles on the grid. In a nutshell, the agent, executing the appropriate action, can move between tiles changing their color upon visiting them. There are 21 positions the agent can be in, four movement actions (left, right, up, and down), one action that simulates the death of the agent bringing it back to the initial position without undoing the coloring that has been done so far. The goal of the agent is to visit every tile in order to color it with the target color. The reward in this abstraction will be 0 for every step except upon succeeding with the task where the reward is 1. This abstraction has 1172830 states, it is

solved through VI, and the ϵ -optimal value function is used to guide the agent through reshaping in the original task. A more detailed description of the abstraction itself and the function $\alpha : \mathcal{S} \rightarrow \bar{\mathcal{S}}$ used to map every state of the original problem into the abstraction’s state space (see Equation 2) are available in Appendix B.2.

5.2.3. ABSTRACTING VENTURE

In the context of *Venture*, the objective of the agent is twofold: exploration to find the rooms’ doors in the main hall; and treasure collection in the rooms. Whenever the agent enters a room, collects its treasure, and exits without being killed, the room gets locked and can no longer be accessed. Therefore, we can define a simple abstraction modeling only the problem of finding the rooms’ doors. This can be done by considering the position of the agent, whether a room is locked or not, the room the agent is currently in, and the boundaries of the main hall. Again, as we did in *Q*Bert*, we will neglect the enemies that chase the agent in the main hall. In the context of the above-described abstraction, visiting a room via one of its doors makes that room transition into the previously-mentioned locked state, hence we are abstracting away what the agent

has to do inside the rooms. The available actions are the movements along the eight main cardinal directions which will change the components of the agent’s positional vector in the appropriate way (increment/decrement by one unit or no change). The goal is to visit all the rooms. When this happens, the agent receives a reward of 1, 0 everywhere else. This abstraction has 106929 states and is again solved ϵ -optimally with VI. The obtained value function is used to do reshaping as stated in Equation 2. The aggregation function is:

$$\alpha(s) = (s_{85}, s_{26}, s_{90}, s_{17}),$$

which means we are considering only the 85th, 26th, 90th, and 17th components (x and y coordinates, room id, and locked rooms, respectively (Anand et al., 2019)) of the original RAM vector.

In the same spirit as the abstraction above, we could build a second layer of abstraction for the rooms within the main hall. Unfortunately, neglecting the monsters there does not allow us to build a good abstraction due to their aggressive behaviour. Indeed, reshaping in these rooms without accounting for the monsters would provide misleading feedback to the agent because the shortest path to the treasure and back out of the room will heavily depend on the enemies’ positions. Neglecting that hinders performance hence, we lean on the agent to find a way to kill the monsters, collect the treasure, and exit. A complete description of the abstraction may be found in Appendix B.3.

5.2.4. RESULTS

In Figures 2b, 2c, and 2d, we report the learning curves associated to the above described algorithms in the context of *Freeway*, *Q*Bert*, and *Venture*, respectively. DQN with fully-connected neural networks and without reshaping is termed DQN, its equivalent version leveraging reshaping through abstraction is called DQN-Reshaped, and DQN based on CNN is called CNN-DQN.

In the context of *Freeway*, as shown in Figure 2b, we observe higher sample efficiency of DQN-Reshaped w.r.t. DQN even though it is not able to achieve the same final performance as CNN-DQN. This fact is due to the usage of a very simplistic abstraction stemming from the assumption of no cars in the road. Unfortunately, accounting for the cars could not be done in the context of this work because of the complex dynamic triggered whenever the agent bumps into a car that could not be reverse engineered from interactions nor from the assembly code.

In *Q*Bert*, Figure 2c, flat fully-connected neural networks when coupled with PBRS and abstractions are able to achieve the same performances of CNNs with approximately one fourth the amount of interactions. Additionally, DQN-Reshaped manages to have the best average perfor-

mance at the end of the learning process.

In the context of *Venture* (see Figure 2d), not only we have greater sample efficiency, but reshaping and abstractions allow fully-connected architectures to achieve the best performance by a great margin w.r.t. all the other solutions.

Finally, the quality of the abstraction, in terms of how well it approximates the original task, plays an important role. Indeed, we can observe a significant difference between the improvement in performance achieved in the context of *Freeway* w.r.t. *Q*Bert* or *Venture*. This is due to the different amount of knowledge provided by a simplistic abstraction compared to a more complex one. Furthermore, the longer the sequence of actions to be executed in order to experience reward, the higher the benefit of reshaping. As a matter of fact, experiencing reward in *Freeway* and *Q*Bert* is quite easy, whereas, in *Venture*, the agent is required to execute a long plan in order to get any positive feedback from the environment. This is reflected by the fact that abstractions in *Venture* provide the best improvement. All the experimental details may be found in Appendix C.³

6. Related Works

Ng et al. (1999) were the first authors to formalize theoretical properties of reward shaping showing that PBRS preserves optimal and near-optimal policies. Wiewiora (2003) proves that, under the same set of collected experience, for Q-learning, SARSA, and other TD-based algorithms, a suitable action-value function initialization is equivalent to PBRS. The first work formally discussing the bias introduced by reshaping when dealing with finite horizons can be found in (Eck et al., 2016). In the context of POMDPs, they show that the evaluation of policies becomes the same as the horizon length tends to infinity. Furthermore, they provide a condition under which two policies, one optimizing the reshaped POMDP and one the original, will be different from each other. This is done to understand when the optimal policy in the finite horizon reshaped POMDP differs from the optimal policy of the original finite horizon POMDP. Our Theorem 4.2, instead, produces a condition to control the bias w.r.t. to the infinite horizon MDP, the true problem of interest. Besides, Theorem 4.1 establishes that, performing reshaping when the horizon is finite does not change the policy ordering w.r.t. the starting finite horizon problem for the goal-oriented case. Grzes̄ (2017), instead, tackle the above-mentioned bias by setting the potential function at the end of the trajectory to zero, hence leveraging non-stationary potential functions (Devlin & Kudenko, 2012).

Along another direction, Cheng et al. (2021) propose a reshaping scheme that leverages the fact that if the poten-

³Code will be made available upon request.

tial was the optimal value function, then a greedily-acting agent would be optimal because all the long-term information would be stored in the potential itself. Therefore, through a mixing coefficient affecting both reshaping and discount factor, the authors propose to solve a curriculum of reshaped MDPs in increasing horizon order. This allows the agent to learn faster because it softens the credit-assignment problem. Furthermore, they learn their potential with offline data using Monte-Carlo Regression.

There is not much theoretical analysis in the literature making explicit the performance improvements attainable with reward shaping. One exception is the work of Gupta et al. (2022), where they provide a regret expression for a new version of UCBVI called UCBVI-Shaped. They assume to have a value function estimator upper-bounding the optimal value function when multiplied by a parameter β (expressing the quality of the estimator itself). This shows that incorporating a good shaping function into exploration bonuses enables a performance improvement that is given by a reduced dependency of the regret on the horizon and state space size. Fully self-supervised reward-shaping techniques (Zheng et al., 2018; Memarian et al., 2021) may not be able to deal with sparse reward settings because they lack an explicit exploration incentive. Therefore, to mitigate this limitation, Devidze et al. (2022) propose to learn an intrinsic reward function combined with a count-based exploration bonus aiming at accelerating the agent’s endeavors in maximizing the extrinsic reward. Along a different direction, Hu et al. (2020) study how to learn the best way to utilize a reshaping function in order to solve the RL problem at hand. They do this through a bi-level optimization approach, where at the first level they optimize the policy to maximize the reshaped rewards, and at the second level they optimize the reshaping function for actual reward maximization.

The work presented in this paper takes also inspiration from abstractions and how they are used in classical planning (Knoblock, 1994). The idea is to automatically build a simplified version of the problem before the search starts. This is obtained by abstracting away all but a (small) part of the task, resulting into a new problem that can be optimally solved fast (Haslum et al., 2007). The plans that solve these abstract problems are then used as heuristics that help guiding the search algorithm toward the goal in the actual problem. Strictly related to the above-mentioned way of using abstractions is the concept of abstractions for MDPs (Congeduti & Frans, 2022). However, as already mentioned in Section 1, they directly employ the solutions obtained from the abstractions onto the real problem. Furthermore, they usually deal with finite state and action MDPs.

Finally, Cipollone et al. (2023) propose an off-policy RL scheme to leverage hierarchies of abstractions and improve

sample efficiency. They mainly focus on goal-oriented MDPs for which they provide a theoretical analysis on the exploration quality of the behavioral policy in their proposed solution that depends on the size of the abstraction state space. This implies that, with sufficiently large abstractions (e.g., in the order of 10^5 states), easily achievable in the context of ALE games (see Section 5), the bound is not helpful. Furthermore, thanks to Theorem 4.1, we can avoid using their off-policy scheme requiring twice the computational complexity to maintain convergence to the optimum. In the context of general MDPs, their approach still represents a sound way to preserve convergence guarantees. However, whenever we cannot afford the computational burden of training two separate agents, thanks to Theorem 4.2, we can try to control the amount of bias we introduce in the reshaped MDP.

7. Conclusions and Future Work

In this paper, we have tackled the problem of sample efficiency in RL through abstraction and PBRS, an idea that was recently introduced in the literature by Cipollone et al. (2023). Contrary to them, we have embraced the bias of PBRS in the context of finite horizons, investigated its effects on policy ordering for goal-oriented and general MDPs, and assessed the contribution to sample efficiency of abstractions coupled with PBRS in highly complex domains such as the ALE benchmark. Given the impressive sample efficiency achieved by the approach, devising ways to learn abstractions automatically from the interactions the agent has with the environment becomes an important avenue for future developments. This could be accomplished by taking inspiration from the HRL literature (Klissarov & Machado, 2023). Furthermore, being able to build abstractions over states spaces represented by images is another interesting future direction for this work that could be pursued through learning an action schema directly from images (Asai & Fukunaga, 2018). Finally, since the idea of using abstraction as a guide to solve the original task is deeply rooted into the planning literature and the concept of heuristics, it would be worthwhile to investigate their connections.

Disclaimer

This paper was prepared for informational purposes by the Artificial Intelligence Research group of JPMorgan Chase & Co. and its affiliates (“JP Morgan”), and is not a product of the Research Department of JP Morgan. JP Morgan makes no representation and warranty whatsoever and disclaims all liability, for the completeness, accuracy or reliability of the information contained herein. This document is not intended as investment research or investment advice, or a recommendation, offer or solicitation for the purchase

or sale of any security, financial instrument, financial product or service, or to be used in any way for evaluating the merits of participating in any transaction, and shall not constitute a solicitation under any jurisdiction or to any person, if such solicitation under such jurisdiction or to such person would be unlawful.

Impact Statement

This paper presents work whose goal is to advance the field of Machine Learning. There are many potential societal consequences of our work, none which we feel must be specifically highlighted here.

References

- Anand, A., Racah, E., Ozair, S., Bengio, Y., Côté, M.-A., and Hjelm, R. D. Unsupervised state representation learning in atari. *Advances in neural information processing systems*, 32, 2019.
- Asai, M. and Fukunaga, A. Classical planning in deep latent space: Bridging the subsymbolic-symbolic boundary. In *Proceedings of the aaai conference on artificial intelligence*, volume 32, 2018.
- Bai, A., Srivastava, S., and Russell, S. Markovian state and action abstractions for mdps via hierarchical mcts. In *IJCAI*, pp. 3029–3039, 2016.
- Bellemare, M. G., Naddaf, Y., Veness, J., and Bowling, M. The arcade learning environment: An evaluation platform for general agents. *Journal of Artificial Intelligence Research*, 47:253–279, 2013.
- Cheng, C.-A., Kolobov, A., and Swaminathan, A. Heuristic-guided reinforcement learning. *Advances in Neural Information Processing Systems*, 34:13550–13563, 2021.
- Cipollone, R., De Giacomo, G., Favorito, M., Iocchi, L., and Patrizi, F. Exploiting multiple abstractions in episodic rl via reward shaping. *Proceedings of the AAAI Conference on Artificial Intelligence*, 37(6):7227–7234, Jun. 2023. doi: 10.1609/aaai.v37i6.25881. URL <https://ojs.aaai.org/index.php/AAAI/article/view/25881>.
- Congeduti, E. and Frans, A. A cross-field review of state abstraction for markov decision processes. In *34th Benelux Conference on Artificial Intelligence (BNAIC) and the 30th Belgian Dutch Conference on Machine Learning (Benelearn)*, 2022.
- D’Eramo, C., Tateo, D., Bonarini, A., Restelli, M., and Peters, J. Mushroomrl: Simplifying reinforcement learning research. *Journal of Machine Learning Research*, 22(131):1–5, 2021. URL <http://jmlr.org/papers/v22/18-056.html>.
- Devdize, R., Kamalaruban, P., and Singla, A. Exploration-guided reward shaping for reinforcement learning under sparse rewards. In *Advances in Neural Information Processing Systems*, 2022.
- Devlin, S. M. and Kudenko, D. Dynamic potential-based reward shaping. In *Proceedings of the 11th international conference on autonomous agents and multiagent systems*, pp. 433–440. IFAAMAS, 2012.
- Eck, A., Soh, L.-K., Devlin, S., and Kudenko, D. Potential-based reward shaping for finite horizon online pomdp planning. *Autonomous Agents and Multi-Agent Systems*, 30:403–445, 2016.
- Givan, R., Leach, S., and Dean, T. Bounded-parameter markov decision processes. *Artificial Intelligence*, 122(1-2):71–109, 2000.
- Grześ, M. Reward shaping in episodic reinforcement learning. In *Proceedings of the 16th Conference on Autonomous Agents and MultiAgent Systems*, pp. 565–573, 2017.
- Gupta, A., Pacchiano, A., Zhai, Y., Kakade, S. M., and Levine, S. Unpacking reward shaping: Understanding the benefits of reward engineering on sample complexity. In *Advances in Neural Information Processing Systems*, 2022.
- Haslum, P., Botea, A., Helmert, M., Bonet, B., Koenig, S., et al. Domain-independent construction of pattern database heuristics for cost-optimal planning. In *AAAI*, volume 7, pp. 1007–1012, 2007.
- Hu, Y., Wang, W., Jia, H., Wang, Y., Chen, Y., Hao, J., Wu, F., and Fan, C. Learning to utilize shaping rewards: A new approach of reward shaping. *Advances in Neural Information Processing Systems*, 33:15931–15941, 2020.
- Hutsebaut-Buysse, M., Mets, K., and Latré, S. Hierarchical reinforcement learning: A survey and open research challenges. *Machine Learning and Knowledge Extraction*, 4(1):172–221, 2022.
- Kingma, D. and Ba, J. Adam: A method for stochastic optimization. In *International Conference on Learning Representations (ICLR)*, San Diego, CA, USA, 2015.
- Klissarov, M. and Machado, M. C. Deep laplacian-based options for temporally-extended exploration. *arXiv preprint arXiv:2301.11181*, 2023.
- Knoblock, C. A. Automatically generating abstractions for planning. *Artificial intelligence*, 68(2):243–302, 1994.

- Lazaric, A. Transfer in reinforcement learning: a framework and a survey. *Reinforcement Learning: State-of-the-Art*, pp. 143–173, 2012.
- LeCun, Y., Bottou, L., Bengio, Y., and Haffner, P. Gradient-based learning applied to document recognition. *Proceedings of the IEEE*, 86(11):2278–2324, 1998.
- Li, L., Walsh, T. J., and Littman, M. L. Towards a unified theory of state abstraction for mdps. In *AI&M*, 2006.
- Memarian, F., Goo, W., Lioutikov, R., Niekum, S., and Topcu, U. Self-supervised online reward shaping in sparse-reward environments. In *2021 IEEE/RSJ International Conference on Intelligent Robots and Systems (IROS)*, pp. 2369–2375. IEEE, 2021.
- Mnih, V., Kavukcuoglu, K., Silver, D., Rusu, A. A., Veness, J., Bellemare, M. G., Graves, A., Riedmiller, M., Fidjeland, A. K., Ostrovski, G., et al. Human-level control through deep reinforcement learning. *nature*, 518(7540):529–533, 2015.
- Ng, A. Y., Harada, D., and Russell, S. Policy invariance under reward transformations: Theory and application to reward shaping. In *Icml*, volume 99, pp. 278–287. Citeseer, 1999.
- OpenAI, Berner, C., Brockman, G., Chan, B., Cheung, V., Debiak, P., Dennison, C., Farhi, D., Fischer, Q., Hashme, S., Hesse, C., Józefowicz, R., Gray, S., Olsson, C., Pachocki, J., Petrov, M., de Oliveira Pinto, H. P., Raiman, J., Salimans, T., Schlatter, J., Schneider, J., Sidor, S., Sutskever, I., Tang, J., Wolski, F., and Zhang, S. Dota 2 with large scale deep reinforcement learning. 2019. URL <https://arxiv.org/abs/1912.06680>.
- Papini, M., Binaghi, D., Canonaco, G., Pirota, M., and Restelli, M. Stochastic variance-reduced policy gradient. In *International conference on machine learning*, pp. 4026–4035. PMLR, 2018.
- Petrik, M. and Subramanian, D. Raam: The benefits of robustness in approximating aggregated mdps in reinforcement learning. *Advances in Neural Information Processing Systems*, 27, 2014.
- Puterman, M. L. *Markov decision processes: discrete stochastic dynamic programming*. John Wiley & Sons, 2014.
- Rummery, G. A. and Niranjan, M. *On-line Q-learning using connectionist systems*, volume 37. University of Cambridge, Department of Engineering Cambridge, UK, 1994.
- Schulman, J., Moritz, P., Levine, S., Jordan, M., and Abbeel, P. High-dimensional continuous control using generalized advantage estimation. *arXiv preprint arXiv:1506.02438*, 2015.
- Silver, D., Hubert, T., Schrittwieser, J., Antonoglou, I., Lai, M., Guez, A., Lanctot, M., Sifre, L., Kumaran, D., Graepel, T., et al. A general reinforcement learning algorithm that masters chess, shogi, and go through self-play. *Science*, 362(6419):1140–1144, 2018.
- Sutton, R. S., McAllester, D., Singh, S., and Mansour, Y. Policy gradient methods for reinforcement learning with function approximation. *Advances in neural information processing systems*, 12, 1999.
- Taylor, M. E. and Stone, P. Transfer learning for reinforcement learning domains: A survey. *Journal of Machine Learning Research*, 10(7), 2009.
- Touati, A., Rapin, J., and Ollivier, Y. Does zero-shot reinforcement learning exist? In *The Eleventh International Conference on Learning Representations*, 2022.
- Vinyals, O., Babuschkin, I., Czarnecki, W. M., Mathieu, M., Dudzik, A., Chung, J., Choi, D. H., Powell, R., Ewalds, T., Georgiev, P., et al. Grandmaster level in starcraft ii using multi-agent reinforcement learning. *Nature*, 575(7782):350–354, 2019.
- Watkins, C. J. and Dayan, P. Q-learning. *Machine learning*, 8:279–292, 1992.
- Wiewiora, E. Potential-based shaping and q-value initialization are equivalent. *Journal of Artificial Intelligence Research*, 19:205–208, 2003.
- Zheng, Z., Oh, J., and Singh, S. On learning intrinsic rewards for policy gradient methods. *Advances in Neural Information Processing Systems*, 31, 2018.

A. Proofs

A.1. Proof of Theorem 4.1

Proof. Let π^* be the optimal policy in the original MDP and $p_\pi(\tau) = \rho(s_0)\pi(a_0|s_0)\prod_{t=1}^{H-1}\mathcal{P}(s_{t+1}|s_t, a_t)\pi(a_t|s_t)$, representing the density of the distribution over the set of all trajectories induced by the policy and the transition dynamics. Then:

$$\mathbb{E}_{\tau \sim p_{\pi^*}} [\mathcal{R}'(\tau)] > \mathbb{E}_{\tau \sim p_\pi} [\mathcal{R}'(\tau)] \quad \forall \pi \neq \pi^* \quad (8)$$

$$\mathbb{E}_{\tau \sim p_{\pi^*}} \left[\mathcal{R}(\tau) + \gamma^{h(\tau)} \phi(s_G) - \cancel{\phi(s_0)} \right] > \mathbb{E}_{\tau \sim p_\pi} \left[\mathcal{R}(\tau) + \gamma^{h(\tau)} \phi(s_h^\pi) - \cancel{\phi(s_0)} \right] \quad \forall \pi \neq \pi^*, \quad (9)$$

where, in (9), we have used $\mathcal{R}'(\tau) = \mathcal{R}(\tau) + \gamma^H \phi(s_H) - \phi(s_0)$ (Grzesiński, 2017), and $h(\tau)$ represents the random variable associated to the horizon length that depends on the policy and environment dynamics. Assuming the potential will be maximal in the goal, then choosing $\pi = \pi^{**}$ (the second-best policy w.r.t. \mathcal{M}) will maximize the right-hand side of the inequality:

$$\mathbb{E}_{\tau \sim p_{\pi^*}} \left[\mathcal{R}(\tau) + \gamma^{h(\tau)} \phi(s_G) \right] > \mathbb{E}_{\tau \sim p_{\pi^{**}}} \left[\mathcal{R}(\tau) + \gamma^{h(\tau)} \phi(s_G) \right]. \quad (10)$$

Now, (10) is always true because:

$$\mathbb{E}_{\tau \sim p_{\pi^*}} [\mathcal{R}(\tau)] > \mathbb{E}_{\tau \sim p_{\pi^{**}}} [\mathcal{R}(\tau)]$$

and

$$\begin{aligned} \mathbb{E}_{\tau \sim p_{\pi^*}} \left[\gamma^{h(\tau)} \phi(s_G) \right] &> \mathbb{E}_{\tau \sim p_{\pi^{**}}} \left[\gamma^{h(\tau)} \phi(s_G) \right] \\ \mathbb{E}_{\tau \sim p_{\pi^*}} \left[\sum_{t=0}^{H-1} \gamma^t r(s_t, a_t, s_{t+1}) \right] &> \mathbb{E}_{\tau \sim p_{\pi^{**}}} \left[\sum_{t=0}^{H-1} \gamma^t r(s_t, a_t, s_{t+1}) \right] \\ \mathbb{E}_{\tau \sim p_{\pi^*}} [\mathcal{R}(\tau)] &> \mathbb{E}_{\tau \sim p_{\pi^{**}}} [\mathcal{R}(\tau)] \end{aligned}$$

Furthermore, iterating this process for any policy starting from the best and the second best up to the ones requiring $H - 1$ and H steps, we see that the ordering is preserved in the reshaped MDP. For what concerns all the other policies requiring more than H steps to achieve the goal, let us restart from 10 selecting π^H instead of π^* , and π^{H+k} for any k instead of π^{**} :

$$\mathbb{E}_{\tau \sim p_{\pi^H}} \left[\mathcal{R}(\tau) + \gamma^H \phi(s_G) \right] > \mathbb{E}_{\tau \sim p_{\pi^{H+k}}} \left[\mathcal{R}(\tau) + \gamma^H \phi(s_H) \right].$$

This inequality is true because $\mathbb{E}_{\tau \sim p_{\pi^H}} [\mathcal{R}(\tau)] > \mathbb{E}_{\tau \sim p_{\pi^{H+k}}} [\mathcal{R}(\tau)] = 0$ and $\phi(s_G) \geq \phi(s_H)$. □

A.2. Proof of Theorem 4.2

Proof. Given the definition of $p_\pi(\tau)$, let $p_\pi^\infty(\tau)$ be its limit for H going to infinity. Furthermore, let $\mathbb{E}_{p_{\pi_A}} [\mathcal{R}'(\tau)]$ and $\mathbb{E}_{p_{\pi_B}} [\mathcal{R}'(\tau)]$ be the performance of two generic policies in the reshaped MDP such that $\mathbb{E}_\rho [V^{\pi_A}(s)] > \mathbb{E}_\rho [V^{\pi_B}(s)]$. Then, for the ordering to be preserved in the reshaped MDP, the following must hold:

$$\begin{aligned} \mathbb{E}_{p_{\pi_A}} [\mathcal{R}'(\tau)] &> \mathbb{E}_{p_{\pi_B}} [\mathcal{R}'(\tau)] \quad \forall \pi_A, \pi_B \\ \mathbb{E}_{p_{\pi_A}} \left[\mathcal{R}(\tau) + \gamma^H \phi(s_H) - \cancel{\phi(s_0)} \right] &> \mathbb{E}_{p_{\pi_B}} \left[\mathcal{R}(\tau) + \gamma^H \phi(s_H) - \cancel{\phi(s_0)} \right] \quad \forall \pi_A, \pi_B \\ \mathbb{E}_{p_{\pi_A}} [\mathcal{R}(\tau)] - \mathbb{E}_{p_{\pi_B}} [\mathcal{R}(\tau)] &> \mathbb{E}_{p_{\pi_B}} [\gamma^H \phi(s_H)] - \mathbb{E}_{p_{\pi_A}} [\gamma^H \phi(s_H)] \quad \forall \pi_A, \pi_B, \end{aligned} \quad (11)$$

where in (11) we have used: $\mathcal{R}'(\tau) = \mathcal{R}(\tau) + \gamma^H \phi(s_H) - \phi(s_0)$.

The potential is bounded, $\phi \in [0, \Phi]$. Hence, given $\mathcal{R}(\tau_H^\infty) = \sum_{t=H}^{\infty} \gamma^t r(s_t, a_t, s_{t+1})$, we have:

$$\begin{aligned} \mathbb{E}_{p_{\pi_A}} [\mathcal{R}(\tau)] - \mathbb{E}_{p_{\pi_B}} [\mathcal{R}(\tau)] &> \gamma^H \Phi \quad \forall \pi_A, \pi_B \\ \mathbb{E}_{p_{\pi_A}} [\mathcal{R}(\tau)] - \mathbb{E}_{p_{\pi_B}} [\mathcal{R}(\tau)] + \mathbb{E}_{p_{\pi_A}^\infty} [\mathcal{R}(\tau_H^\infty)] - \mathbb{E}_{p_{\pi_B}^\infty} [\mathcal{R}(\tau_H^\infty)] &> \gamma^H \Phi + \mathbb{E}_{p_{\pi_A}^\infty} [\mathcal{R}(\tau_H^\infty)] - \mathbb{E}_{p_{\pi_B}^\infty} [\mathcal{R}(\tau_H^\infty)] \\ \mathbb{E}_\rho [V^{\pi_A}(s)] - \mathbb{E}_\rho [V^{\pi_B}(s)] &> \gamma^H \Phi + \mathbb{E}_{p_{\pi_A}^\infty} [\mathcal{R}(\tau_H^\infty)] \\ \mathbb{E}_\rho [V^{\pi_A}(s)] - \mathbb{E}_\rho [V^{\pi_B}(s)] &> \gamma^H \Phi + \frac{\gamma^H}{1-\gamma} \bar{R} \\ \gamma^H &< \inf_{\substack{\pi_A, \pi_B: \\ \mathbb{E}_\rho [V^{\pi_A}(s)] > \mathbb{E}_\rho [V^{\pi_B}(s)]}} \frac{\mathbb{E}_\rho [V^{\pi_A}(s)] - \mathbb{E}_\rho [V^{\pi_B}(s)]}{\Phi + \frac{\bar{R}}{1-\gamma}} \\ H &> \log_{\gamma} \inf_{\substack{\pi_A, \pi_B: \\ \mathbb{E}_\rho [V^{\pi_A}(s)] > \mathbb{E}_\rho [V^{\pi_B}(s)]}} \frac{\mathbb{E}_\rho [V^{\pi_A}(s)] - \mathbb{E}_\rho [V^{\pi_B}(s)]}{\Phi + \frac{\bar{R}}{1-\gamma}} \end{aligned}$$

□

B. Abstractions

B.1. Grid World

In this section, we describe the 8-rooms abstraction, reported as a graph in Figure 3. Each node is associated to a room with the topology of the graph and the coloring faithfully representing Figure 1 (this also defines the aggregation function). The connections between nodes are bidirectional and represent the available actions. Additionally, any action has a 90% chance of success and a 10% failure probability. This means that, with probability 0.9, the agent ends up into the intended target node, with probability 0.1, instead, it will stay where it is. Closely following Cipollone et al. (2023), this stochastic behavior is implemented in the original 8-rooms environment of Figure 1 as well, but, in this case, the agent has a 4% failure probability upon executing any action, and, when it fails, one among all the available actions is executed at random.

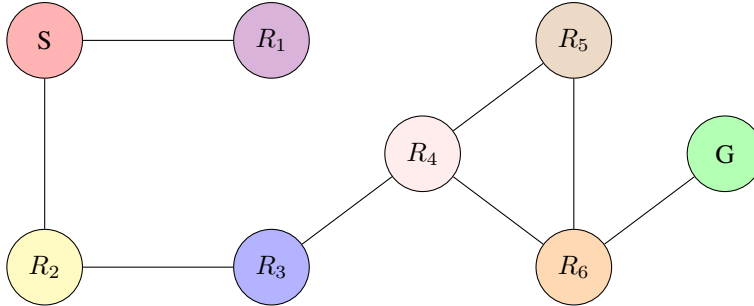


Figure 3: Grid World abstraction.

B.2. Q*Bert

B.2.1. THE ABSTRACTION

The nodes in Figure 4 represent the tiles the agent has to color. The agent starts at tile 1 that has coordinates $(77, 25)$ (see Table 1) and it can move according to the connections reported in the graph of Figure 4. For instance, if the agent is at node 5, it can move to 3 by executing the *up* action, it can move to 2 by executing *left*, it can move to 9 by executing *right*, it can move to 8 by executing *down*, and, finally, it can *die* there by moving back directly to 1. To avoid cluttering, the dying action has been reported only for node 6 in Figure 4, it applies to all the nodes, and it does not change the color of the landing tile (which is always 1). All the other movement actions will change the color of the landing tile and they have been reported only for node 5 for the sake of readability (the pattern is the same for every node except for the borders where missing arcs mean that the associated actions are not available for execution). The state space of the abstraction is then represented by the x and y coordinates of the agent corresponding to the coordinates reported in Table 1 and 21 variables representing the colors of the tiles that start all at the same source color and need to be transitioned all to the target by the

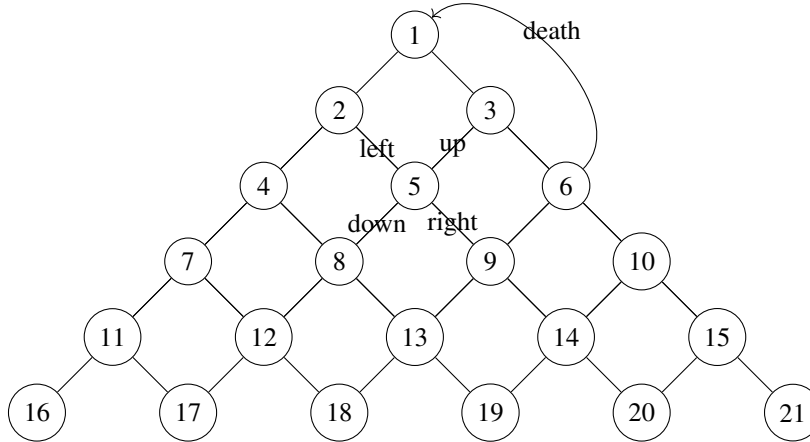


Figure 4: Q*Bert Transition Graph. The Node ID correspond to the position in x, y coordinates reported in Table 1.

agent. Formally, being s the state vector of the original task, we have:

$$\begin{aligned} \bar{s} &= (s_{43}, s_{67}, s_{21}, s_{52}, s_{54}, s_{83}, s_{85}, s_{87}, s_{98}, s_{100}, s_{102}, s_{104}, s_1, s_3, s_5, s_7, s_9, s_{32}, s_{34}, s_{36}, s_{38}, s_{40}, s_{42}) \\ &= (\underbrace{x, y}_{\text{Coordinates}}, \underbrace{1, 2, 3, 4, 5, 6, 7, 8, 9, 10, 11, 12, 13, 14, 15, 16, 17, 18, 19, 20, 21}_{\text{Node IDs reported in Figure 4}}) \end{aligned}$$

Table 1: Node ID to position mapping.

Node ID	(x, y)	Node ID	(x, y)
1	(77, 25)	12	(53, 137)
2	(65, 53)	13	(77, 137)
3	(93, 53)	14	(105, 137)
4	(53, 81)	15	(129, 137)
5	(77, 81)	16	(16, 165)
6	(105, 81)	17	(41, 165)
7	(41, 109)	18	(65, 165)
8	(65, 109)	19	(93, 165)
9	(93, 109)	20	(117, 165)
10	(117, 109)	21	(141, 165)
11	(29, 137)		

B.2.2. THE COLORING ACROSS DIFFERENT LEVELS

In the context of the original task, on every level, we have a different source-target color pair that can be detected automatically at the first few interactions of the agent with the new level. This is done by monitoring the transitions the agent is experiencing. Whenever we go to a new level (57^{th} component of the RAM vector), we grab the color of tile 1, then as soon as we transition from 1 to either 2 or 3 and the color of one of those two tiles has changed w.r.t. the one we grabbed in 1 we save the source-target color pair. This automatic mechanism allows us to make our abstraction agnostic to the color change across different levels, so that the abstraction is kept fixed throughout the whole learning process and does not depend on the level the agent is at. Finally, notice that, handling all possible different source-target color pairs not only enables us to have a single abstraction for all the levels, but it also enables a pre-processing step that translate all the source-target color pairs into a single one to help the network better leverage similarities across levels. In Figure 2c, we have reported results using abstraction and pre-processing combined, whereas in Figure 5, we report an ablation study to better asses the contribution of the single components: only abstraction and only pre-processing. As we may see, with reshaping we are able to greatly improve performances w.r.t. the basic DQN solution. The same may be stated for what concerns leveraging

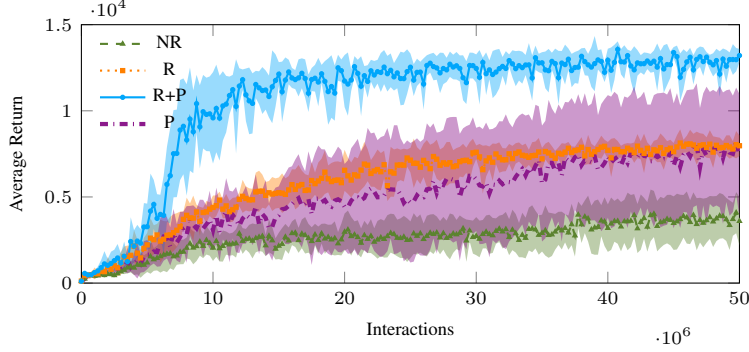


Figure 5: Average return achieved by simple fully-connected DQN without Reshaping (NR), with Reshaping (R), with Pre-processing (P), with Reshaping and Pre-processing (R+P) ± 1 standard deviation computed using 10 independent runs in Q^*Bert .

the pre-processing at the cost of a greater variance. The two techniques combined yield the best performance surpassing even CNN-based DQN as stated in Section 5.2.4.

B.2.3. THE AGGREGATION FUNCTION

In order to complete the map between \mathcal{S} and $\bar{\mathcal{S}}$, we need to account for the transition dynamics between the nodes connected via the actions *up*, *right*, *down*, and *left* in Figure 4.⁴ In our abstraction that transition is instantaneous, but in the real task it is not. Let us see an example:

$$\underbrace{(77, 25)}_{\bar{s}_{x,y}^1}, \underbrace{(78, 24), (82, 20), (86, 22), (89, 27), (89, 35), (89, 43), (89, 51), (93, 53)}_{\bar{s}_{x,y}^2}.$$

This represents the transitions undergone by the x and y coordinates of the agent when moving from tile 1 to tile 3 in the original task. This is the same transition, but at level 2:

$$\underbrace{(77, 25)}_{\bar{s}_{x,y}^1}, \underbrace{(81, 21), (85, 21), (89, 25), (89, 33), (89, 41), (89, 49), (93, 53)}_{\bar{s}_{x,y}^2}.$$

Furthermore, to make things even harder, they keep on changing throughout the various different levels. Since this transition is mandatory, and the agent cannot deviate from it, we are going to define the aggregation function taking the endpoints as representatives and assigning the in-between states as shown above. Formally, let $\sigma_1, \dots, \sigma_k = \sigma \in \varsigma$ be a possible sequence of succeeding x and y coordinates allowed by the game between $(77, 25)$ and $(93, 53)$, then the aggregation function for this family of transitions will map $(77, 25) \rightarrow (77, 25)$ and $\{\sigma, (93, 53)\} \rightarrow (93, 53) \forall \sigma \in \varsigma$, and so on for every other node in Figure 4. In order to induce the above described partitioning, we are going to use the action chosen by the agent. Indeed, given the agent is at $(77, 25)$, if it executes the action *right*, it will observe the appropriate $\sigma \in \varsigma$ and then, eventually, $(93, 53)$. This implies that we are able to properly reshape between $(77, 25)$ and the first x and y coordinate pair, σ_1 , in the σ sequence. The reshaping of all the other transitions, namely, $\langle \sigma_2, \sigma_3 \rangle, \dots, \langle \sigma_k, (93, 53) \rangle$, are set to 0.

The pseudo-code that shows an implementation of the F function (see Section 2.1) for Q^*Bert is shown in Algorithm 1, where we are assuming that \mathcal{G} is a hash-map representing the transition graph reported in Figure 4 without the death arcs. \mathcal{V}_ϵ is the solution produced by VI applied to the abstraction. Finally, the function `next_state`, given the current abstract state and the x and y coordinates the agents ends up at after executing a , returns the abstract next state by appropriately coloring the required tile in \bar{s} . In Line 1, we do not reshape if the starting state coordinates are out of our abstraction. In Line 5 we do not reshape if the agent stays still, this is done not to incentive continuous movement. In Lines 8 to 13, if the agent moved out of the abstraction from a known state, we penalize it with $-\phi(s)$. This is because it is jumping out of the grid and consequently dying. Otherwise, if the state is unknown, we don't reshape (Line 12). In Line 14, we handle the

⁴Note that this mapping induce a partition over the original state space where each \bar{s} is a class representative.

Algorithm 1 Q*Bert F function

```

1: Input:  $\langle \bar{s}, a, \bar{s}' \rangle$  the transition,  $\mathcal{G}$  the abstraction's transition graph,  $\phi = \mathcal{V}_\epsilon$  the potential function
2: if  $\bar{s}_{x,y}$  not in  $\mathcal{G}$  then
3:   return 0
4: end if
5: if  $\bar{s}_{x,y} == \bar{s}'_{x,y}$  then
6:   return 0
7: end if
8: if  $a$  not in  $\mathcal{G} [s]$  then
9:   if  $\bar{s}$  in  $\phi$  then
10:    return  $-\phi(\bar{s})$ 
11:   else
12:    return 0
13:   end if
14: else if  $\bar{s}$  in  $\phi$  and  $\text{next\_state}(\bar{s}, \mathcal{G} [\bar{s}_{x,y}] [a])$  in  $\phi$  then
15:    $F = \gamma\phi(\text{next\_state}(\bar{s}, \mathcal{G} [\bar{s}_{x,y}] [a])) - \phi(\bar{s})$ 
16:   if  $F==0$  then
17:    return 0.1
18:   end if
19:   return  $F$ 
20: else
21:   return 0
22: end if

```

transition between one abstract tile and another. If the value of F is 0 we boost it to 0.1 (this happens every time we take an action that is optimal according to \mathcal{V}_ϵ), otherwise, we simply return F .⁵ In all other remaining cases 0 is returned.

Changing the reshaping function like we have described above deviates from theory and it may introduce bias, but as we have seen in the experiments of Figure 2c the achieved performance is better than CNN-based DQN. Additionally, it is worth noticing that, in Algorithm 1, for the sake of readability, we did not report the pseudo-code to handle all the possible source-target color pairs. Finally, we normalize the reward of the original task dividing it by 500 (the highest reward obtainable in a single step). This does not change the task from the optimization point of view and make everything in a similar scale w.r.t. reshaping values.

B.3. Venture

Table 2: Main hall door to room door position mapping

Main Hall Door	Action	Room Door
(65, 62)	<i>left</i>	(129, 63)
(36, 34)	<i>bottom</i>	(58, 11)
(112, 50)	<i>up</i>	(62, 18)
(145, 48)	<i>left</i>	(129, 13)
(141, 10)	<i>left</i>	(129, 15)
(88, 9)	<i>right</i>	(31, 15)
(54, 14)	<i>left</i>	(117, 39)
(20, 18)	<i>right</i>	(43, 39)

In Figure 6, we may find a complete description of the main-hall abstraction with all the rooms, the obstacles, and, in red, the doors to access the rooms. The agent starts in position (68, 76). Furthermore, notice that, whenever we are over a door position by playing the appropriate action we will enter the room and end up over the corresponding door position on the other side. For instance, if the agent is at (65, 62) by playing the action *left* it will end up being at (129, 63) in Room 1

⁵Notice that our abstraction is a goal-oriented MDP solved with the same discount factor used in the original task, see Section C.

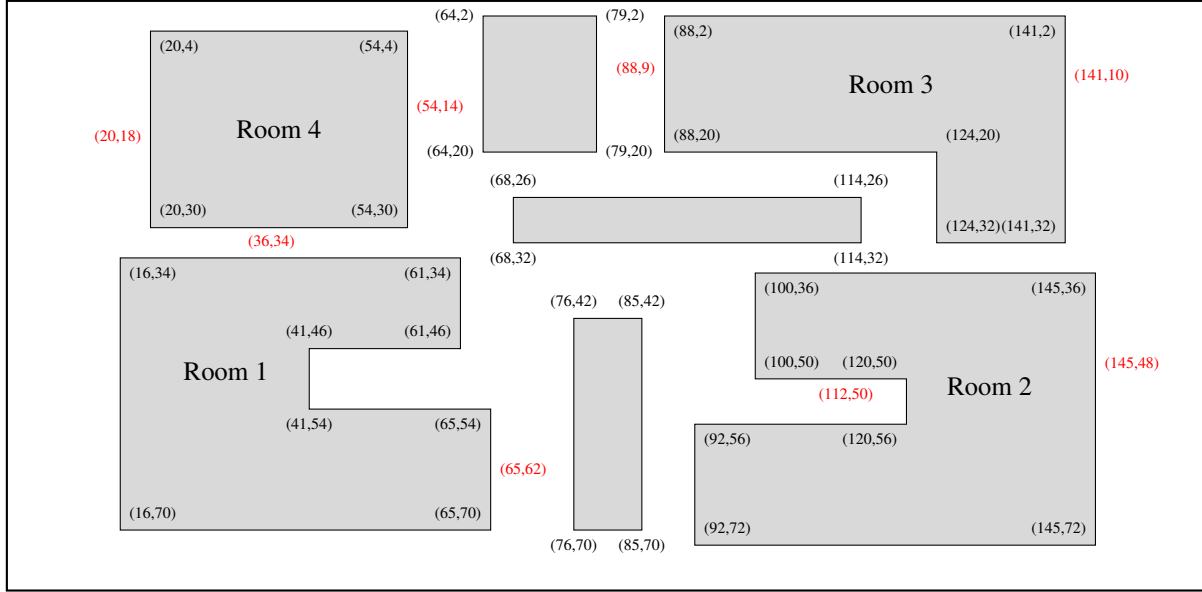


Figure 6: Venture abstraction: main hall.

(see Table 2). From there, the agent will only be able to go back by playing *right* effectively locking the room, as if it was solved. In Algorithm 2, we report the pseudo-code describing an implementation of the reshaping mechanism in the context of *Venture*. Here, the only potential sources of bias are due to Line 3 of Algorithm 2, where we return 0 if the agent stays still to avoid incentives to continuous movement, and in Algorithm 3, where we return 0 if one of the two abstract state is out of the abstraction. This was done because during preliminary experimental studies it appeared to give better performances.

Algorithm 2 Venture F function

- 1: **Input:** $\langle s, a, s' \rangle$ the transition, $\phi^0 = \mathcal{V}_\epsilon^0$ the potential function associated to the main hall
 - 2: **if** $s_{85,26} == s'_{85,26}$ **then**
 - 3: **return** 0
 - 4: **end if**
 - 5: **if** $s_{90} == 8$ **then**
 - 6: **return** $F_8(s, a, s', \phi^0)$
 - 7: **end if**
 - 8: **return** 0
-

Algorithm 3 Venture F_8 function

- 1: **Input:** $\langle s, a, s' \rangle$ the transition, $\phi = \mathcal{V}_\epsilon^0$ the potential function associated to the main hall
 - 2: $\bar{s} = s_{85,26,90,17}$, $\bar{s}' = s'_{85,26,90,17}$
 - 3: **if** \bar{s} in ϕ and \bar{s}' in ϕ **then**
 - 4: $F = \gamma\phi(\bar{s}') - \phi(\bar{s})$
 - 5: **return** $10^3 F$
 - 6: **end if**
 - 7: **return** 0
-

C. Experimental Details

C.1. Value Iteration

In this section, we will describe all the configurations of the VI algorithm employed to solve the above-described abstractions. For all the abstractions we have an ϵ of 10^{-7} , whereas the discount factor γ is 0.98 for *Freeway* and *Venture*, 0.99 for *Q*Bert*, and 0.9 for the Grid World.

C.2. Deep Q-Networks

For what concerns the ALE benchmark, we used Mushroom-RL (D’Eramo et al., 2021) implementation of DQN with the hyperparameters reported in Table 3. Notice that, for *Freeway* the **test exploration rate** has been lowered to 0.01 because yielded better performance in evaluation for the CNN architecture. Furthermore, being *Freeway* a very simple task to solve, we lowered **evaluation frequency** to 100000 and the **test samples** to 50000. This enables a more frequent probing of the agent performance that allows a higher resolution for the learning curve, which, in turn, allows us to better visualize and understand the learning dynamic especially in the early epochs, where it matters the most.

Adam (Kingma & Ba, 2015) is used as optimizer with learning rate to 0.0001 and $(\beta_1, \beta_2) = (0.9, 0.999)$. In the case of RAM states, we have fully-connected neural networks with the following structure: one input layer of $128 \cdot 4$ neurons, two hidden layers of 128 and 256 neurons (first and second hidden layers, respectively) both with ReLU activation functions, and an output layer whose size depends on the number of actions (*Freeway* has 3, *Q*Bert* 6, and *Venture* 18). In the case of image states, instead, we have an input shape of (4, 84, 84) and the CNN structure is the following: 3 convolutional layers and 2 linear layers. The first convolutional layer has 4 input channels, 32 output channels, a kernel size of 8, and stride of 4; the second one has 32 input channels, 64 output channels, a kernel size of 4, and stride of 2; the third one has 64 input channels, 64 output channels, a kernel size of 3, and stride of 1. The first linear layer has 3136 neurons and the second 512. The output is the number of actions that depends on the task and it is already stated above. Every layer has a ReLU activation function except the output layer that does not have any.

Table 3: DQN Hyperparameters

Parameter	Value	Description
γ	0.99	The discount factor
initial replay size	50000	Initial number of samples in the replay memory
max replay size	500000	Replay memory max capacity
batch size	32	Number of samples for each fit of the network
history Length	4	Number of frames a state is made of
target update frequency	10000	Number of collected samples before a new update of the target network
train frequency	4	Number of collected samples before a new fit of the neural network
final exploration frame	1000000	The number of samples while the exploration rate decays
initial exploration rate	1	The initial exploration rate value
final exploration rate	0.1	The final exploration rate value
max no-op actions	30	Maximum amount of no-ops executed at the beginning of each episode
max steps	50000000	Total number of interactions
evaluation frequency	250000	Total number of interactions before evaluating the policy
test samples	125000	Interactions during policy evaluation
test exploration rate	0.05	Exploration rate used while evaluating the policy

C.3. Q-Learning

In this section, we report all the hyperparameters used to train Q-Learning in the context of the 8-rooms task. The parameter δ starts at 0.5 and it decays to 0.01, the parameter ϵ of the ϵ -greedy policy starts at 1 and it decays to 0.1, both of them in 300000 time steps (the whole learning process). Finally, we have an episode maximum length of 70 and a discount factor of 0.98.